International Journal of Electrochemical Science 19 (2024) 100558

Contents lists available at ScienceDirect

International Journal of Electrochemical Science

journal homepage: www.editorialmanager.com/ijoes

Robust equivalent circuit model parameters identification scheme for State of Charge (SOC) estimation based on maximum correntropy criterion

Kexin Zhang[a,b,c,1], Xuezhuan Zhao[a,b,c,*,2], Yu Chen[a,b,c,3], Di Wu[d,4], Taotao Cai[d,5], Yi Wang[a,b,c,6], Lingling Li[e,**,7], Ji Zhang[d,8]

[a] School of Intelligent Engineering, Zhengzhou University of Aeronautics, Zhengzhou, Henan 450046, China
[b] Collaborative Innovation Center of Aeronautics and Astronautics Electronic Information Technology, Zhengzhou, Henan 450046, China
[c] Henan Key Laboratory of General Aviation Technology, Zhengzhou, Henan 450046, China
[d] School of Mathematics, Physics and Computing, University of Southern Queensland, Toowoomba, Queensland 4350, Australia
[e] Zhengzhou University of Aeronautics, Zhengzhou, Henan 450046, China

ARTICLE INFO

Keywords:
Battery management system
Equivalent circuit model
Robust parameters identification
Maximum correntropy criterion

ABSTRACT

Equivalent circuit model (ECM) parameters identification, which aims to identify the model parameters of ECM accurately is vital for assessing battery status and refining battery management systems (BMS), extensive research has been conducted in this field. However, most of the existing studies rely on global similarity criteria such as Root Mean Square Error (RMSE) and Sum of Squares due to Error (SSE), which are highly sensitive to non-Gaussian noise, so they may not perform effectively when faced with the non-Gaussian noise which is often encountered in battery working environments. This article presents a robust ECM parameter identification scheme termed the Maximum Correntropy Criterion-based Gradient Ascending scheme (MCCGA). The proposed MCCGA scheme adopts correntropy for similarity assessment and leverages a gradient ascent algorithm to optimize the model parameters iteratively. Through these methods, the MCCGA scheme not only identifies model parameters with precision but also remains robustness to non-Gaussian noise. Extensive experimental results based on public dataset are provided, which validate the effectiveness, robustness and convergence of the proposed MCCGA scheme.

1. Introduction

In recent years, the popularity of new energy vehicles has skyrocketed due to their cost-effectiveness and eco-friendly features. As a crucial component in these vehicles, lithium-ion batteries have gained widespread usage. Despite their numerous advantages, such as high energy density, reusability, and long lifespan, lithium batteries can be susceptible to instability, including risks of explosion or fire, especially when exposed to extreme conditions like ultra-high/low temperatures or overcharge/discharge situations. Therefore, enhancing the safety and reliability of lithium-ion batteries becomes imperative. The Battery Management System (BMS) plays a pivotal role in maintaining the proper function of batteries and prolonging their lifespan and many research works [1–5] have been done to improve the performance of BMS. A well-designed and efficient BMS ensures that the battery operates under optimal conditions and maximizes its service life. The most important function of the BMS is to detect various parameters of the battery while effectively controlling its operational status.

* Corresponding author at: School of Intelligent Engineering, Zhengzhou University of Aeronautics, Zhengzhou, Henan 450046, China.
** Corresponding author.
E-mail addresses: zhaoxuezhuan@zua.edu.cn (X. Zhao), lilingling@zua.edu.cn (L. Li).
[1] 0009-0001-7557-2615
[2] 0009-0002-3801-4638
[3] 0009-0009-1250-5798
[4] 0000-0002-4753-8161
[5] 0000-0002-3624-6120
[6] 0000-0003-3833-4287
[7] 0000-0002-1147-512X
[8] 0000-0001-7167-6970

https://doi.org/10.1016/j.ijoes.2024.100558
Received 18 February 2024; Received in revised form 17 March 2024; Accepted 21 March 2024
Available online 24 March 2024

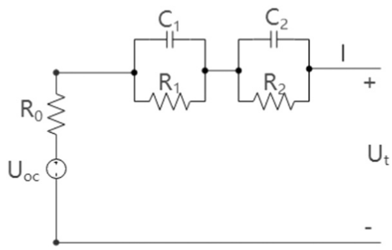

Fig. 1. Second-order RC model.

Among all the battery parameters, the State of Charge (SOC), which indicates the remaining available power within the battery, holds utmost significance and plays a pivotal role in BMS. However, the SOC information could not be measured directly and can only be estimated based on the battery's voltage, current, ambient temperature, and other information. In this context, efficient and accurate estimation of the battery's State of Charge (SOC) is particularly important. Currently, the SOC estimation methods can be divided into three categories: traditional methods [1,6], data-driven methods [2,7–10,11], and model-based methods [3,12–15,16]. The Coulomb Counting method is the most classic method for SOC estimation and has high accuracy in a short time. However, this method relies on the accuracy of initial values and suffers from accumulated errors. Another traditional method is the Open Circuit Voltage(OCV) based method, which utilizes the OCV-SOC curve to estimate the SOC. Although this method is easy to understand, it requires a long time to ensure the accuracy of OCV, making it unsuitable for real-time applications. Data-driven methods mainly use various neural networks to obtain the nonlinear relationship between measurable data (current, voltage, ambient temperature, etc.) and SOC, and then use the trained neural network to predict SOC. [17] used a deep neural network (DNN) to map the battery measurements to SOC and achieved good performance. [18] developed a recurrent neural network (RNN) with long short-term memory (LSTM) to estimate the SOC, which got accurate estimation at different ambient temperature. [19] proposed a network which combined convolutional neural network (CNN) and LSTM network together to exploit the relationship between the measurable data and SOC. [2] presented the DAE-NN network which combined a denoising autoencoder neural network(DAE-NN) and a gated recurrent unit recurrent neural network (GRU-RNN) to estimate the SOC and get accurate estimation. Although data-driven methods can exploit the nonlinear relationship between measurable data and SOC, they often require a vast amount of training data and bring significant computational burdens. The model-based methods combine the equivalent circuit model (ECM) with various kinds of adaptive filters to estimate SOC, [20] proposed a method based on a nonlinear battery model and an extended Kalman filter (EKF) to accurately estimate SOC. [21] developed a co-estimation method which utilized the unscented Kalman filter(UKF) to estimate SOC. Also, some improved methods [22–24] based on EKF and UKF have been presented to improve estimation accuracy. The model based methods eliminate the need for extensive training data and can be executed in real-time, making them widely adopted in practical applications. However, the estimation accuracy of model-based methods heavily relies on the chosen equivalent circuit model and its associated parameters. Hence, it is vital to carefully select an appropriate ECM model and conduct accurate parameter identification.

Currently, the main equivalent circuit models include Rint, Thevenin, PNGV, and Second-order RC model, among others. [25,26]. The first three models have straightforward structures and are easy to deploy. However, they are not accurate enough. On the other hand, the Second-order RC model, depicted in Fig. 1, has moderate complexity and can accurately describe the polarization process of the battery, making it the most widely used equivalent circuit model at present. Within the Second-order RC model, five model parameters need to be identified,

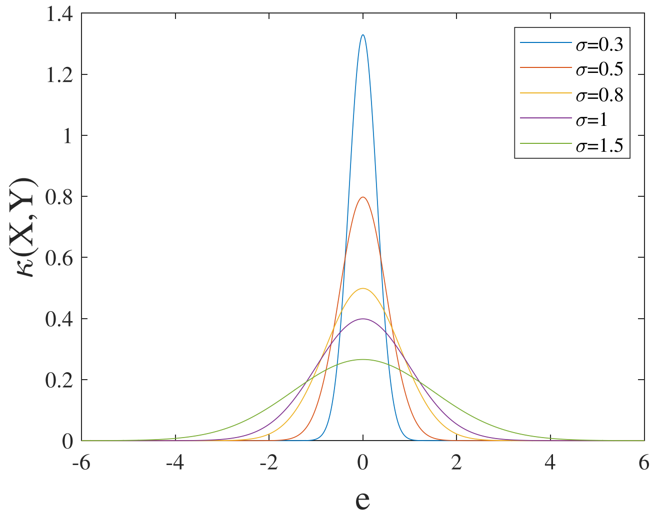

Fig. 2. Gaussian kernel function with varying σ.

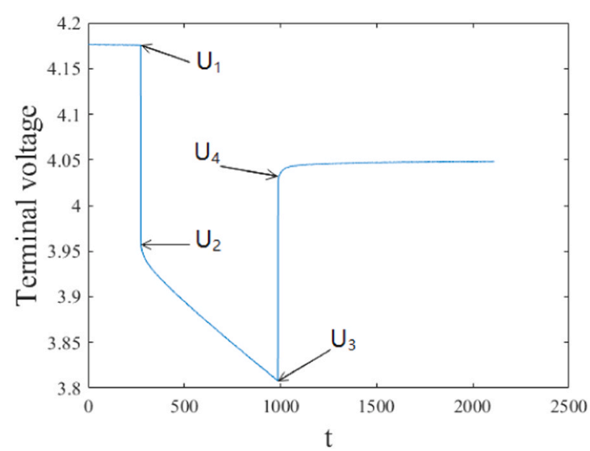

Fig. 3. Terminal voltage U_t during one cycle.

namely ohmic resistance R_0, polarization resistances R_1, R_2, and polarization capacitances C_1, C_2. Accurately identifying these model parameters is critical for characterizing battery status and optimizing BMS. In this context, numerous methods [27–30,31] for parameter identification have been proposed to accomplish accurate model parameter identification. However, most of them are based on global similarity criteria such as RMSE and SSE, which are highly sensitive to non-Gaussian noise. Consequently, these methods may lack robustness regarding parameter identification in environments with non-Gaussian noise, which is commonly encountered in battery working conditions. Therefore, when the battery measurement data is contaminated by non-Gaussian noise, these parameter identification methods may not yield reliable results. To address the challenges posed by non-Gaussian noise, this paper introduces a robust ECM parameter identification scheme MCCGA based on the maximum correntropy criterion (MCC) [32,33]. By utilizing the maximum correntropy as the similarity measurement criterion and employing the maximum gradient descent method, the MCCGA scheme enables accurate identification of ECM parameters while remaining robust to non-Gaussian noise. The effectiveness and robustness of the proposed MCCGA scheme are demonstrated through experimental results using public datasets. The contributions of this article can be summarized as follows:

1. We propose a robust ECM parameter identification scheme MCCGA based on the maximum correntropy criterion (MCC). The MCCGA

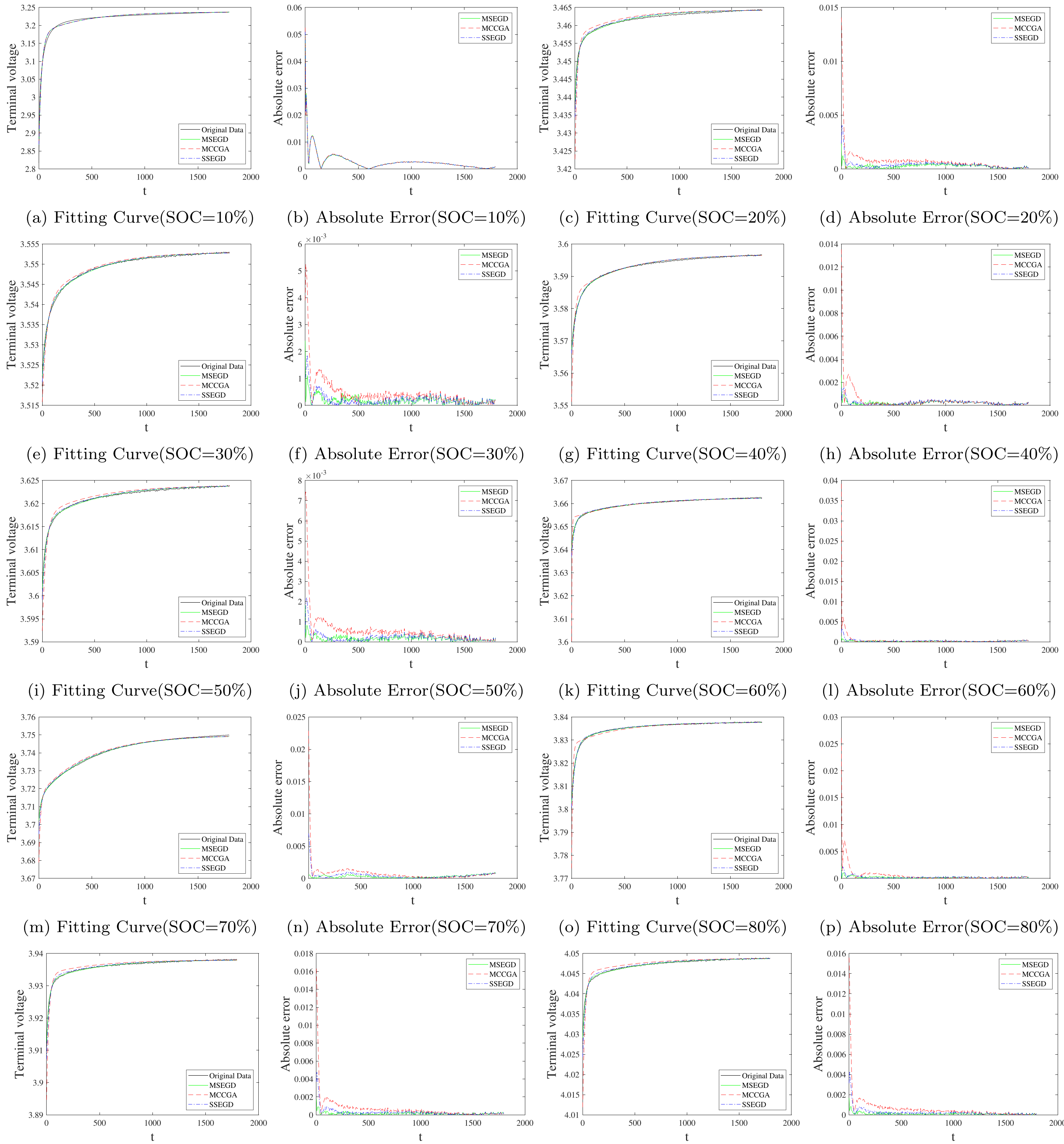

(a) Fitting Curve(SOC=10%) (b) Absolute Error(SOC=10%) (c) Fitting Curve(SOC=20%) (d) Absolute Error(SOC=20%)
(e) Fitting Curve(SOC=30%) (f) Absolute Error(SOC=30%) (g) Fitting Curve(SOC=40%) (h) Absolute Error(SOC=40%)
(i) Fitting Curve(SOC=50%) (j) Absolute Error(SOC=50%) (k) Fitting Curve(SOC=60%) (l) Absolute Error(SOC=60%)
(m) Fitting Curve(SOC=70%) (n) Absolute Error(SOC=70%) (o) Fitting Curve(SOC=80%) (p) Absolute Error(SOC=80%)
(q) Fitting Curve(SOC=90%) (r) Absolute Error(SOC=90%) (s) Fitting Curve(SOC=100%) (t) Absolute Error(SOC=100%)

Fig. 4. Effectiveness under different SOC.

scheme not only identifies the model parameters with precision but also is robust to non-Gaussian noise.

2. We give the object function of the proposed MCCGA scheme and derive the iterative optimization rules to identify the optimal model parameters;
3. Extensive experimental results across various SOC states based on public datasets are provided, which demonstrate the effectiveness, robustness, and convergence of the proposed MCCGA scheme;

The rest of this paper is organized as follows: Section 2 provides an overview of the relevant works. Section 3 gives a detailed description of the proposed MCCGA scheme. Extensive experimental results based on public datasets are presented in Section 4. Finally, Section 5 concludes the paper.

Table 1
Performance metric results of MCCGA under different SOC.

SOC	MAE	MSE	RMSE
SOC = 10%	0.0027	2.24E-05	0.0047
SOC = 20%	7.10E-04	1.98E-06	0.0014
SOC = 30%	4.50E-04	5.93E-07	7.7E-04
SOC = 40%	4.27E-04	1.37E-06	0.0012
SOC = 50%	5.54E-04	9.96E-07	9.98E-04
SOC = 60%	4.13E-04	4.86E-06	0.0022
SOC = 70%	7.64E-04	3.35E-06	0.0018
SOC = 80%	5.7E-04	3.31E-06	0.0018
SOC = 90%	6.7E-04	2.44E-06	0.0016
SOC = 100%	5.99E-04	2.12E-06	0.0015

2. Related works

2.1. Maximum correntropy criterion (MCC)

Correntropy [32–34], as a method for measuring similarity, is capable of describing the similarity between two random variables. Unlike global similarity criteria such as RMSE and SSE, which are sensitive to non-Gaussian noise, correntropy is a local similarity measurement criterion that exhibits robustness to non-Gaussian noise, particularly when it comes to impulse noise. Hence, correntropy proves to be reliable in a non-Gaussian environment.The correntropy of random variables X and Y can be expressed using Formula (1):

$$V(X,Y)=E[\kappa(X,Y)] \tag{1}$$

In Formula (1), the symbol $E[\cdot]$ represents the expected value, and $\kappa(\cdot)$ denotes the kernel function that maps variables from low-dimensional space to high-dimensional space. Among various kernel functions, the Gaussian kernel function is the most widely used kernel function.Its expression is illustrated by Formula (2)

$$\begin{aligned}\kappa(X,Y) &= \frac{1}{\sqrt{2\pi}\sigma}\exp\left(\frac{-\parallel X-Y\|^2}{2\sigma^2}\right)\\ &= \frac{1}{\sqrt{2\pi}\sigma}\exp\left(-\frac{e^2}{2\sigma^2}\right)\end{aligned} \tag{2}$$

In Formula (2), $e=X-Y$ represents the difference between X and Y, and σ corresponds to the kernel width, which influences the suppression strength on outliers(usually impulse noise). Fig. 1 displays the curves of Gaussian kernel functions for varying values of σ. From Fig. 1, we can deduce that:

1. The function value exhibits an inverse relationship with the value of $|X-Y|$. As $|X-Y|$ increases, the function value decreases. Consequently, this function possesses a strong ability to suppress outliers;
2. The more similar X and Y are, the larger the function value is. When $X = Y$, the function value reaches its maximum. Thus, maximizing the function value is needed to minimize the difference between X and Y;
3. The suppression effect of the function on outliers becomes more prominent as the value of σ decreases, and vice versa.

The joint probability distribution of variables X and Y is typically unknown. Consequently, we usually approximate the correntropy of $X = \{x_0, x_1, x_2, \ldots, x_M\}$ and $Y = \{y_0, y_1, y_2, \ldots, y_M\}$ using Formula (3), where M denotes the number of samples of the variable X and YFig. 2.

$$V(X,Y)=\frac{1}{M}\sum_{i=1}^{M}\kappa(x_i,y_i) \tag{3}$$

2.2. Second-order RC model

The Second-order RC model [25,26,30], depicted in Fig. 1, is the most widely used equivalent circuit model. In order to get the accurate model parameters (R_0, R_1, R_2, C_1, C_2), we usually first charge the battery to the setting threshold using constant current and constant voltage, then discharge the battery for ten cycles. During each cycle, the electrical energy equivalent to 10% of SOC is discharged using constant current first, and then the battery is left standing for a period of time. The terminal voltage of each cycle is recorded to identify the model parameters. The terminal voltage U_t during one cycle is illustrated in Fig. 3. From Fig. 3 we can see that:

1. When the battery starts to discharge at a constant current I, the terminal voltage jumps from U_1 to U_2, and When the battery stops discharging, the terminal voltage jumps from U_3 to U_4. These jumps are caused by the ohmic resistance R_0, hence the model parameter R_0 can be calculated using Formula (4);

$$R_0=\frac{U_1-U_2+U_4-U_3}{2I} \tag{4}$$

2. When the battery stops discharging, the terminal voltage firstly jumps from U_3 to U_4 and then gradually increases to a fixed value, which can be considered as the open circuit voltage U_{oc} at this stage. The gradually increasing process of the terminal voltage U_t during this stage is caused by the second-order RC circuit and can be expressed using Formula (5);

$$U_t=U_{oc}-U_{RC1}\exp\left(-\frac{t}{R_1C_1}\right)-U_{RC2}\exp\left(-\frac{t}{R_2C_2}\right) \tag{5}$$

In Formula (5), U_{oc} represents the open circuit voltage,while U_{RC1} and U_{RC2} denote the voltages on the RC1 and RC2 branches, respectively.The values of U_{RC1} and U_{RC2} can be expressed by Formula (6) and Formula (7);

$$U_{RC1}=IR_1 \tag{6}$$

$$U_{RC2}=IR_2 \tag{7}$$

To identify the model parameters R_1, R_2, C_1, C_2, various kinds of curve fitting methods have been proposed. However, most of these methods rely on global similarity criteria such as RMSE, SSE, etc., which are sensitive to non-Gaussian noise. Hence, they are not robust to the non-Gaussian noise, especially impulse noise. In light of this, we introduce a robust parameter identification scheme MCCGA, based on the maximum correntropy criterion (MCC), in Section 2.1 to improve the robustness of the parameters identification process. The MCCGA scheme will be described in detail in Section 3.

3. MCC based parameters identification scheme MCCGA

To address the challenges posed by non-Gaussian noise, we propose a parameter identification scheme MCCGA based on the maximum correntropy criterion (MCC) in this section. In the MCCGA scheme, correntropy is used as the similarity measurement standard, and a gradient ascending algorithm is employed to optimize the model parameters iteratively. By maximizing the correntropy, we can obtain the optimal model parameters. Here we give the MCC-based object function according to Formula (3) and Formula (2).

$$OBJ_{MCC}=\frac{1}{M}\sum_{i=1}^{M}\frac{1}{\sqrt{2\pi}\sigma}\exp\left(\frac{-\left(U_t^{pred}-U_t\right)^2}{2\sigma^2}\right) \tag{8}$$

In Formula (8), U_t represents the actual measured terminal voltage at time point t, while U_t^{pred} corresponds to the predicted terminal voltage by Formula (5) at time point t. Thus, the object function can be expressed in detail as Formula (9).

$$OBJ_{MCC} = \frac{1}{M}\sum_{t=1}^{M}\frac{1}{\sqrt{2\pi}\sigma}\exp\left(\frac{-\left(U_{oc} - U_{RC1}\exp\left(-\frac{t}{R_1C_1}\right) - U_{RC2}\exp\left(-\frac{t}{R_2C_2}\right) - U_t\right)^2}{2\sigma^2}\right) \quad (9)$$

So the optimization problem can be formulated as Formula (10):In

$$\begin{aligned}\{U_{RC1},\theta_1,U_{RC2},\theta_2\} &= \operatorname{argmax}_{U_{RC1},\theta_1,U_{RC2},\theta_2} OBJ_{MCC} \\ &= \operatorname{argmax}_{U_{RC1},\theta_1,U_{RC2},\theta_2}\frac{1}{M}\sum_{t=1}^{M}\frac{1}{\sqrt{2\pi}\sigma}\exp\left(\frac{-\left(U_{oc} - U_{RC1}\exp\left(-\frac{t}{\theta_1}\right) - U_{RC2}\exp\left(-\frac{t}{\theta_2}\right) - U_t\right)^2}{2\sigma^2}\right)\end{aligned} \quad (10)$$

Formula (10), $\theta_1 = R_1C_1$, $\theta_2 = R_2C_2$.To find the maximum value of the objective function OBJ_{MCC}, we employ the gradient ascent algorithm. Firstly, we compute the gradients of the objective function with respect to each variable(U_{RC1}, θ_1, U_{RC2}, θ_2), the gradients for each variable are expressed by Formula (11), (12), (13), (14)

$$\frac{\partial OBJ_{MCC}}{\partial U_{RC1}} = -\frac{1}{M}\sum_{t=1}^{M}\frac{\exp\left(-\frac{f^2(U_{RC1},\theta_1,U_{RC2},\theta_2)}{2\sigma^2}\right)\exp(-t/\theta_1)f(U_{RC1},\theta_1,U_{RC2},\theta_2)}{\sqrt{2\pi}\sigma^3} \quad (11)$$

$$\frac{\partial OBJ_{MCC}}{\partial \theta_1} = -\frac{1}{M}\sum_{t=1}^{M}\frac{U_{RC1}t\exp\left(-\frac{f^2(U_{RC1},\theta_1,U_{RC2},\theta_2)}{2\sigma^2}\right)\exp(-t/\theta_1)f(U_{RC1},\theta_1,U_{RC2},\theta_2)}{\sqrt{2\pi}\theta_1^2\sigma^3} \quad (12)$$

$$\frac{\partial OBJ_{MCC}}{\partial U_{RC2}} = -\frac{1}{M}\sum_{t=1}^{M}\frac{\exp\left(-\frac{f^2(U_{RC1},\theta_1,U_{RC2},\theta_2)}{2\sigma^2}\right)\exp(-t/\theta_2)f(U_{RC1},\theta_1,U_{RC2},\theta_2)}{\sqrt{2\pi}\sigma^3} \quad (13)$$

$$\frac{\partial OBJ_{MCC}}{\partial \theta_2} = -\frac{1}{M}\sum_{t=1}^{M}\frac{U_{RC2}t\exp\left(-\frac{f^2(U_{RC1},\theta_1,U_{RC2},\theta_2)}{2\sigma^2}\right)\exp(-t/\theta_2)f(U_{RC1},\theta_1,U_{RC2},\theta_2)}{\sqrt{2\pi}\theta_2^2\sigma^3} \quad (14)$$

In the Formulas, function $f(U_{RC1}, \theta_1, U_{RC2})$ is defined as follows (15)

$$f(U_{RC1},\theta_1,U_{RC2},\theta_2) = U + U_{RC1}\exp(-t/\theta_1) + U_{RC2}\exp(-t/\theta_2) - U_{oc} \quad (15)$$

Consequently, we derive the iterative optimization rules for each variable based on the gradient ascent algorithm, as presented by Formula (16), (17), (18), (19)

$$U_{RC1}^{t+1} = U_{RC1}^{t} + lr\frac{\partial OBJ_{MCC}}{\partial U_{RC1}} \quad (16)$$

$$\theta_1^{t+1} = \theta_1^{t} + lr\frac{\partial OBJ_{MCC}}{\partial \theta_1} \quad (17)$$

$$U_{RC2}^{t+1} = U_{RC2}^{t} + lr\frac{\partial OBJ_{MCC}}{\partial U_{RC2}} \quad (18)$$

$$\theta_2^{t+1} = \theta_2^{t} + lr\frac{\partial OBJ_{MCC}}{\partial \theta_2} \quad (19)$$

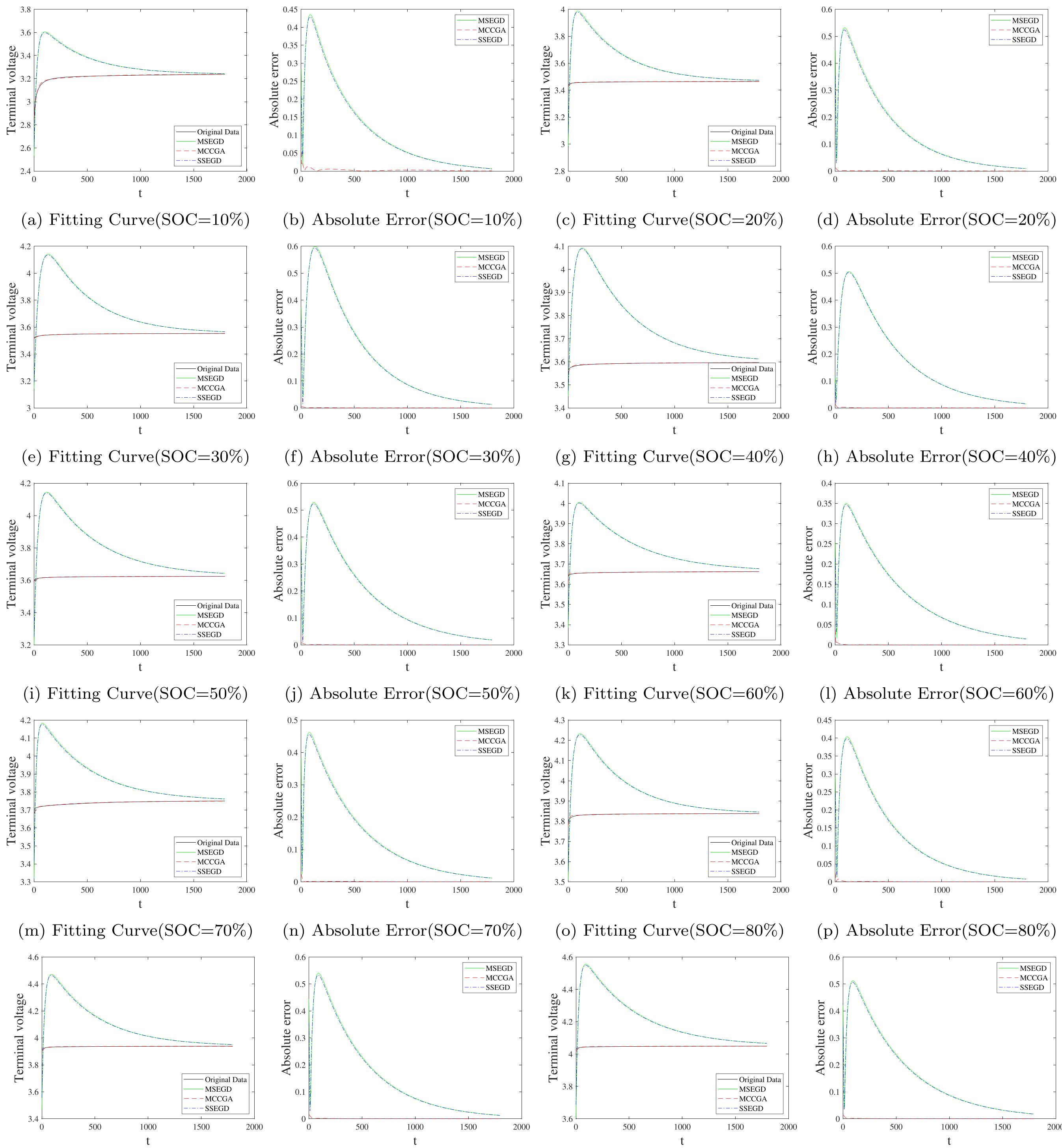

(a) Fitting Curve(SOC=10%) (b) Absolute Error(SOC=10%) (c) Fitting Curve(SOC=20%) (d) Absolute Error(SOC=20%)

(e) Fitting Curve(SOC=30%) (f) Absolute Error(SOC=30%) (g) Fitting Curve(SOC=40%) (h) Absolute Error(SOC=40%)

(i) Fitting Curve(SOC=50%) (j) Absolute Error(SOC=50%) (k) Fitting Curve(SOC=60%) (l) Absolute Error(SOC=60%)

(m) Fitting Curve(SOC=70%) (n) Absolute Error(SOC=70%) (o) Fitting Curve(SOC=80%) (p) Absolute Error(SOC=80%)

(q) Fitting Curve(SOC=90%) (r) Absolute Error(SOC=90%) (s) Fitting Curve(SOC=100%) (t) Absolute Error(SOC=100%)

Fig. 5. Robustness under different SOC.

In Formula (16), (17), (18), (19),lr denotes the learning rate which controls the learning speed. After a certain number of iterations, we can obtain the optimal values of the variables(U_{RC1}, θ_1, U_{RC2}, θ_2) and subsequently calculate the corresponding battery model parameters(R_1, R_2, C_1, C_2). The MCCGA scheme is summarized in Algorithm 1.

Algorithm 1. MCCGA

```
Input: Terminal voltage U under different SOC, discharge current I, initial value of
       U_RC1, θ1, U_RC2, θ2, learning rate lr, kernel width σ;
Output: The identified model parameters R1, R2, C1, C2.
  repeat
    Update U_RC1 by Formula 16;
    Update θ1 by Formula 17;
    Update U_RC2 by Formula 18;
    Update θ2 by Formula 19;
  until Convergence
  Calculate R1 by R1 = U_RC1/I;
  Calculate R2 by R2 = U_RC2/I;
  Calculate C1 by C1 = θ1/R1;
  Calculate C2 by C2 = θ2/R2;
  return R1, R2, C1, C2
```

Detailed experimental results are provided in Section 4.

4. Experiment result

In this section, we used the public dataset of INR 18650–20R battery[9] for our experiment. The battery was initially charged to its maximum capacity of 100% SOC and then discharged at every 10% SOC using a negative pulse current of 1A for ten cycles. In each cycle, after the discharge process, the battery was left standing for a period of time. At this stage, the terminal voltage U_t gradually increased to a fixed value. Usually, the better we fit the gradually increasing process of the terminal voltage U_t in each cycle by Formula (5), the more accurate the model parameters identification will be. Here, the kernel width σ was set to be 1, MAE(Mean absolute error) [36], MSE(Mean square error) [36,37], and RMSE(Root MSE) [36] which are described in Equations (20), (21), (22) respectively were utilized as the performance evaluation metrics to test the fitting errors, in the equations, N is the number of sample points, Y_m is the ground truth value, $Y^*{}_m$ is the predicted value.

$$MAE = \frac{1}{N}\sum_{m=1}^{N}\left|Y_m - Y^*{}_m\right| \tag{20}$$

$$MSE = \frac{1}{N}\sum_{m=1}^{N}\left(Y_m - Y^*{}_m\right)^2 \tag{21}$$

$$RMSE = \sqrt{\frac{1}{N}\sum_{m=1}^{N}\left(Y_m - Y^*{}_m\right)^2} \tag{22}$$

The experimental results based on Algorithm 1 are provided from three aspects: 1)Effectiveness, the experimental results under the original terminal voltage data are given, which demonstrate the effectiveness of the MCCGA scheme; 2)Robustness, the experimental results under the terminal voltage data contaminated by non-Gaussian noise are provided to illustrate the robustness of MCCGA scheme.3)Convergence, the values of objection function OBJ_{MCC} are given to prove the convergence of the MCCGA scheme. Here, the SSE [36] based gradient descent (SSEGD) algorithm and MSE [36,37] based gradient descent(MSEGD) algorithm are used as the baselines for comparison.

4.1. Effectiveness

Here, we first utilized the MCCGA scheme to derive the model parameters of the Second-order RC model based on the original terminal voltage data. Specifically, we only used the data in the first 30 min, as after standing for 30 min, the terminal voltage had already been stable. Subsequently, we employed the second-order RC model with the model parameters identified using Algorithm 1 to predict the terminal voltage. The predicted results under different SOC using MCCGA are depicted in Fig. 4a, c, e, g, i, k, m, o, q, s, also the predicted results based on SSEGD and MSEGD, the original terminal voltage curve are shown in the same figures, it can be observed that the predicted results based on MCCGA, SSEGD and MSEGD all fit well with the original data curves. Furthermore, the absolute error curves for MCCGA, SSEGD and MSEGD are shown in Fig. 4b, d, f, h, j, l, n, p, r, t, showing that the absolute errors based on MCCGA, SSEGD and MSEGD are very small, particularly, the performance metric results of MCCGA under different SOC are given in Table 1. All of these demonstrate the effectiveness of the MCCGA scheme.

4.2. Robustness

In order to demonstrate the robustness of the MCCGA scheme, we conducted experiments using terminal voltage data contaminated by non-Gaussian noise. The noise is composed of Gaussian noise and shot noise [35]. Here, we adopt the same experimental steps as when verifying the effectiveness of the MCCGA scheme. The predicted results for different SOC using MCCGA scheme are presented in Fig. 5a, c, e, g, i, k, m, o, q, s, also the predicted results based on SSEGD and MSEGD, the original terminal voltage curve are shown in the same figures. The absolute error curves for MCCGA, SSEGD and MSEGD are shown in Fig. 5b, d, f, h, j, l, n, p, r, t. From Fig. 5, it can be observed that the proposed MCCGA algorithm performs well even when the terminal voltage data is contaminated by non-Gaussian noise, with the predicted error still very small. On the other hand, the SSEGD and MSEGD algorithms both fail to work correctly on datasets contaminated by non-Gaussian noise. In particular, the performance metric results of MCCGA across various SOC on datasets contaminated by non-Gaussian noise are given in Table 2, which demonstrate the robustness of the proposed MCCGA scheme. This is attributed to the fact that the MCCGA scheme adopts correntropy as

[9] https://calce.umd.edu/battery-data

Table 2
Performance metric results of MCCGA on datasets contaminated by non-Gaussian noise under different SOC.

SOC	MAE	MSE	RMSE
SOC = 10%	0.0027	2.24E-05	0.0047
SOC = 20%	8.2E-04	1.82E-06	0.0013
SOC = 30%	4.89E-04	6.33E-07	7.95E-04
SOC = 40%	5.24E-04	1.61E-06	0.0013
SOC = 50%	5.19E-04	9.43E-07	9.71E-04
SOC = 60%	4.19E-04	4.64E-06	0.0022
SOC = 70%	8.13E-04	3.72E-06	0.0019
SOC = 80%	5.98E-04	3.09E-06	0.0018
SOC = 90%	6.33E-04	2.29E-06	0.0015
SOC = 100%	5.8E-04	1.93E-06	0.0014

the similarity measurement standard, which has a strong ability to suppress outliers.

4.3. Convergence

The convergence curves are presented in Fig. 6. In the figure, the x-axis represents the number of iterations, and y-axis represents the value of OBJ_{MCC}, which is the object function of the MCCGA scheme. From Fig. 6, it can be observed that the value of the OBJ_{MCC} is monotonically nondecreasing under rules (16), (17), (18), (19), which prove that the object function OBJ_{MCC} is convergent under the update rules (16), (17), (18), (19).

5. Conclusion

In this paper, we propose the MCCGA scheme, a robust parameter identification scheme for ECM based on MCC. The proposed MCCGA is capable of accurately identifying model parameters while also robust to non-Gaussian noise. The MCCGA scheme adopts correntropy for similarity assessment and leverages a gradient ascent algorithm to optimize the model parameters iteratively. Extensive experimental results based on public datasets are presented to demonstrate the effectiveness, robustness, and convergence of the proposed MCCGA scheme. In the future, our research will focus on developing more accurate and robust ECM parameter identification scheme.

CRediT authorship contribution statement

Kexin Zhang: Conceptualization, Data curation, Methodology, Resources, Writing – original draft. **Xuezhuan Zhao:** Software, Supervision, Visualization, Writing – review & editing. **Taotao Cai:** Validation. **Yi Wang:** Software. **Yu Chen:** Formal analysis, Investigation. **Di Wu:** Software, Validation. **Lingling Li:** Funding acquisition, Project administration, Writing – review & editing. **Ji Zhang:** Writing – review & editing.

Declaration of Competing Interest

The authors declare that they have no known competing financial interests or personal relationships that could have appeared to influence the work reported in this paper.

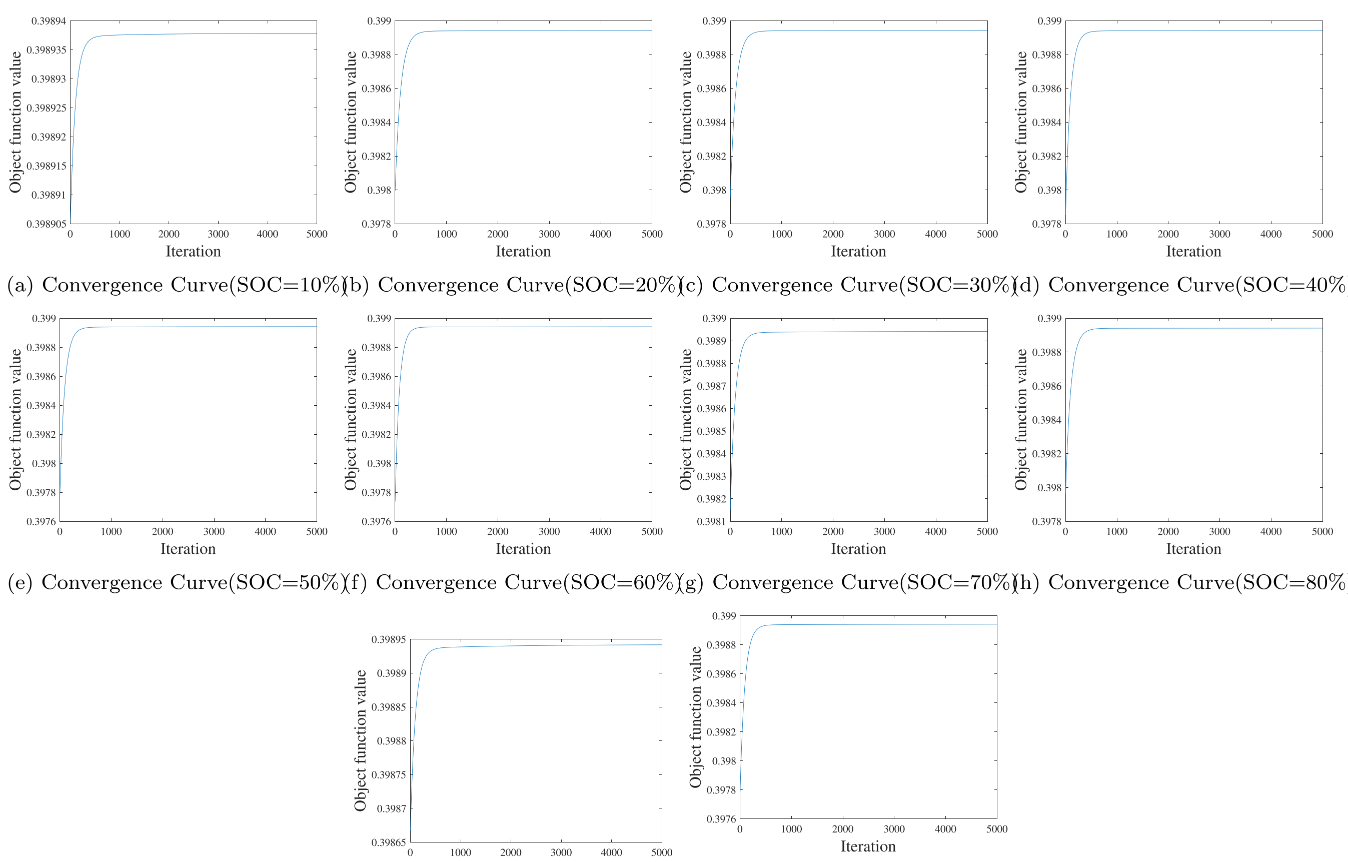

(a) Convergence Curve(SOC=10%) (b) Convergence Curve(SOC=20%) (c) Convergence Curve(SOC=30%) (d) Convergence Curve(SOC=40%)

(e) Convergence Curve(SOC=50%) (f) Convergence Curve(SOC=60%) (g) Convergence Curve(SOC=70%) (h) Convergence Curve(SOC=80%)

(i) Convergence Curve(SOC=90%) (j) Convergence Curve(SOC=100%)

Fig. 6. Convergence under different SOC.

Acknowledgments

The authors thank the associate editor and the anonymous reviewers for their constructive comments and suggestions. This work was partially supported by the Scientific and Technological Key Project of Henan Province (232102241003, 232102210054), the Henan Center for Outstanding Overseas Scientists (GZS2022011), the Training Program for Young Scholar of Henan Province for Colleges and Universities (2020GGJS172), Henan Key Laboratory of General Aviation Technology.

References

[1] X. Chen, H. Lei, R. Xiong, W. Shen, R. Yang, A novel approach to reconstruct open circuit voltage for state of charge estimation of lithium ion batteries in electric vehicles, Appl. Energy 255 (2019) 113758, https://doi.org/10.1016/j.apenergy.2019.113758.

[2] J. Chen, X. Feng, L. Jiang, Q. Zhu, State of charge estimation of lithium-ion battery using denoising autoencoder and gated recurrent unit recurrent neural network, Energy 227 (2021) 120451, https://doi.org/10.1016/j.energy.2021.120451.

[3] R. Xiong, W. Shunli, Y. Chunmei, X. Lili, An estimation method for lithium-ion battery soc of special robots based on Thevenin model and improved extended Kalman, Energy Storage Sci. Technol. 10 (2) (2021) 695, https://doi.org/10.19799/j.cnki.2095-4239.2020.0397.

[4] S. Wang, Y. Fan, S. Jin, P. Takyi-Aninakwa, C. Fernandez, Improved anti-noise adaptive long short-term memory neural network modeling for the robust remaining useful life prediction of lithium-ion batteries, Reliab. Eng. Syst. Saf. 230 (2023) 108920, https://doi.org/10.1016/j.ress.2022.108920.

[5] S. Wang, F. Wu, P. Takyi-Aninakwa, C. Fernandez, D.-I. Stroe, Q. Huang, Improved singular filtering-gaussian process regression-long short-term memory model for whole-life-cycle remaining capacity estimation of lithium-ion batteries adaptive to fast aging and multi-current variations, Energy 284 (2023) 128677, https://doi.org/10.1016/j.energy.2023.128677.

[6] J.P. Rivera-Barrera, N. Muñoz-Galeano, H.O. Sarmiento-Maldonado, Soc estimation for lithium-ion batteries: Review and future challenges, Electronics 6 (4) (2017) 102, https://doi.org/10.3390/electronics6040102.

[7] M.S.H. Lipu, M.A. Hannan, A. Hussain, M.H. Saad, A. Ayob, M.N. Uddin, Extreme learning machine model for state-of-charge estimation of lithium-ion battery using gravitational search algorithm, IEEE Trans. Ind. Appl. 55 (4) (2019) 4225–4234, https://doi.org/10.1109/TIA.2019.2902532.

[8] J. Chen, Q. Ouyang, C. Xu, H. Su, Neural network-based state of charge observer design for lithium-ion batteries, IEEE Trans. Control Syst. Technol. 26 (1) (2017) 313–320, https://doi.org/10.1109/TCST.2017.2664726.

[9] X. Wang, Q. Sun, X. Kou, W. Ma, H. Zhang, R. Liu, Noise immune state of charge estimation of li-ion battery via the extreme learning machine with mixture generalized maximum correntropy criterion, Energy 239 (2022) 122406, https://doi.org/10.1016/j.energy.2021.122406.

[10] D.N. How, M.A. Hannan, M.S.H. Lipu, K.S. Sahari, P.J. Ker, K.M. Muttaqi, State-of-charge estimation of li-ion battery in electric vehicles: a deep neural network approach, IEEE Trans. Ind. Appl. 56 (5) (2020) 5565–5574, https://doi.org/10.1109/TIA.2020.3004294.

[11] C. Bian, H. He, S. Yang, T. Huang, State-of-charge sequence estimation of lithium-ion battery based on bidirectional long short-term memory encoder-decoder architecture, J. Power Sources 449 (2020) 227558, https://doi.org/10.1016/j.jpowsour.2019.227558.

[12] Q. Yu, R. Xiong, C. Lin, W. Shen, J. Deng, Lithium-ion battery parameters and state-of-charge joint estimation based on h-infinity and unscented Kalman filters, IEEE Trans. Veh. Technol. 66 (10) (2017) 8693–8701, https://doi.org/10.1109/TVT.2017.2709326.

[13] K.-T. Lee, M.-J. Dai, C.-C. Chuang, Temperature-compensated model for lithium-ion polymer batteries with extended Kalman filter state-of-charge estimation for an implantable charger, IEEE Trans. Ind. Electron. 65 (1) (2017) 589–596, https://doi.org/10.1109/TIE.2017.2721880.

[14] P. Guo, W. Ma, D. Yi, X. Liu, X. Wang, L. Dang, Enhanced square root ckf with mixture correntropy loss for robust state of charge estimation of lithium-ion battery, J. Energy Storage 73 (2023) 108920, https://doi.org/10.1016/j.est.2023.108920.

[15] Y. Gao, X. Zhang, B. Guo, C. Zhu, J. Wiedemann, L. Wang, J. Cao, Health-aware multiobjective optimal charging strategy with coupled electrochemical-thermal-aging model for lithium-ion battery, IEEE Trans. Ind. Inform. 16 (5) (2020) 3417–3429, https://doi.org/10.1109/TII.2019.2935326.

[16] Y. Li, B. Xiong, D.M. Vilathgamuwa, Z. Wei, C. Xie, C. Zou, Constrained ensemble Kalman filter for distributed electrochemical state estimation of lithium-ion batteries, IEEE Trans. Ind. Inform. 17 (1) (2021) 240–250, https://doi.org/10.1109/TII.2020.2974907.

[17] E. Chemali, P.J. Kollmeyer, M. Preindl, A. Emadi, State-of-charge estimation of li-ion batteries using deep neural networks: a machine learning approach, J. Power Sources 400 (2018) 242–255, https://doi.org/10.1016/j.jpowsour.2018.06.104.

[18] E. Chemali, P.J. Kollmeyer, M. Preindl, R. Ahmed, A. Emadi, Long short-term memory networks for accurate state-of-charge estimation of li-ion batteries, IEEE Trans. Ind. Electron. 65 (8) (2017) 6730–6739, https://doi.org/10.1109/TIE.2017.2787586.

[19] X. Song, F. Yang, D. Wang, K.-L. Tsui, Combined CNN-LSTM network for state-of-charge estimation of lithium-ion batteries, IEEE Access 7 (2019) 88894–88902, https://doi.org/10.1109/ACCESS.2019.2926517.

[20] Z. Chen, Y. Fu, C.C. Mi, State of charge estimation of lithium-ion batteries in electric drive vehicles using extended Kalman filtering, IEEE Trans. Veh. Technol. 62 (3) (2012) 1020–1030, https://doi.org/10.1109/TVT.2012.2235474.

[21] R. Zhu, B. Duan, J. Zhang, Q. Zhang, C. Zhang, Co-estimation of model parameters and state-of-charge for lithium-ion batteries with recursive restricted total least squares and unscented Kalman filter, Appl. Energy 277 (2020) 115494, https://doi.org/10.1016/j.apenergy.2020.115494.

[22] Y. Li, C. Wang, J. Gong, A multi-model probability soc fusion estimation approach using an improved adaptive unscented Kalman filter technique, Energy 141 (2017) 1402–1415, https://doi.org/10.1016/j.energy.2017.11.079.

[23] R. Xiong, H. He, F. Sun, K. Zhao, Evaluation on state of charge estimation of batteries with adaptive extended Kalman filter by experiment approach, IEEE Trans. Veh. Technol. 62 (1) (2012) 108–117, https://doi.org/10.1109/TVT.2012.2222684.

[24] S. Zhang, X. Guo, X. Zhang, An improved adaptive unscented Kalman filtering for state of charge online estimation of lithium-ion battery, J. Energy Storage 32 (2020) 101980, https://doi.org/10.1016/j.est.2020.101980.

[25] S.M. Mousavi, G.M. Nikdel, Various battery models for various simulation studies and applications, Renew. Sustain. Energy Rev. 32 (2014) 477–485, https://doi.org/10.1016/j.rser.2014.01.048.

[26] B. SHH, G. EE, Pngv Battery Test Manual, 1999, 10.2172/578702.

[27] X. Lai, W. Gao, Y. Zheng, M. Ouyang, J. Li, X. Han, L. Zhou, A comparative study of global optimization methods for parameter identification of different equivalent circuit models for li-ion batteries, Electrochim. Acta 295 (2019) 1057–1066, https://doi.org/10.1016/j.electacta.2018.11.134.

[28] S.S. Madani, E. Schaltz, S.K. Kær, A review of different electric equivalent circuit models and parameter identification methods of lithium-ion batteries, ECS Trans. 87 (1) (2018) 23, https://doi.org/10.1149/08701.0023ecst.

[29] N. Tian, Y. Wang, J. Chen, H. Fang, On parameter identification of an equivalent circuit model for lithium-ion batteries, in: Proceedings of the IEEE Conference on Control Technology and Applications (CCTA), IEEE, 2017, pp. 187-192. 10.1109/CCTA.2017.8062461.

[30] X. Hu, S. Li, H. Peng, A comparative study of equivalent circuit models for li-ion batteries, J. Power Sources 198 (2012) 359–367, https://doi.org/10.1016/j.jpowsour.2011.10.013.

[31] S. Jiang, A parameter identification method for a battery equivalent circuit model, Tech. Rep., SAE Technical Paper, 2011, 10.4271/2011-01-1367.

[32] B. Chen, J.C. Príncipe, Maximum correntropy estimation is a smoothed map estimation, IEEE Signal Process. Lett. 19 (8) (2012) 491–494, https://doi.org/10.1109/LSP.2012.2204435.

[33] W. Liu, P.P. Pokharel, J.C. Principe, Correntropy: properties and applications in non-gaussian signal processing, IEEE Trans. Signal Process. 55 (11) (2007) 5286–5298, https://doi.org/10.1109/TSP.2007.896065.

[34] S. Zhao, B. Chen, J.C. Principe, Kernel adaptive filtering with maximum correntropy criterion, in: Proceedings of the International Joint Conference on Neural Networks, IEEE, 2011, pp. 2012–2017. 10.1109/IJCNN.2011.6033473.

[35] M.V. Kulikova, One-step condensed forms for square-root maximum correntropy criterion Kalman filtering, in: Proceedings of the 23rd International Conference on System Theory, Control and Computing (ICSTCC), IEEE, 2019, pp. 13–18. 10.1109/ICSTCC.2019.8885950.

[36] A. Botchkarev, Performance Metrics (Error Measures) in Machine Learning Regression, Forecasting and Prognostics: Properties and Typology, arXiv preprint arXiv:1809.03006, 2018. 10.48550/arXiv.1809.03006.

[37] T.O. Hodson, T.M. Over, S.S. Foks, Mean squared error, deconstructed, J. Adv. Model. Earth Syst. 13 (12) (2021) e2021MS002681, https://doi.org/10.1029/2021MS002681.